Effect of particles on ultraviolet light penetration in natural and engineered systems

Hadas Mamane, Joel J. Ducoste, and Karl G. Linden

The effect of light scattering on measurement of UV absorbance and penetration of germicidal UVC irradiance in a UV reactor were studied. Using a standard spectrophotometer, absorbance measurements exhibited significant error when particles that scatter light were present but could be corrected by integrating sphere spectroscopy. Particles from water treatment plants and wastewater effluents exhibited less scattering (20%–30%) compared with particles such as clay (50%) and alumina (95%–100%). The distribution of light intensity in a UV reactor for a scattering suspension was determined using a spherical chemical actinometry method. Highly scattering alumina particles increased the fluence rate in the reactor near the UV lamp, whereas clay particles and absorbing organic matter reduced the fluence rate. A radiative transfer fluence rate model reasonably predicted the fluence rate of absorbing media and highly scattering suspensions in the UV reactor. © 2006 Optical Society of America

OCIS codes: 290.5820, 300.1030.

1. Introduction

The presence of particles in water confounds the determination of UV disinfection efficiency. Because of unique absorbance and scattering properties, particles interfere with the measurement of UV absorbance, determination of the fluence rate, and the mathematical modeling of UV disinfection systems. Thus improved understanding of the absorbance and scattering properties of particles will lead to advances in areas of fluence rate measurement and modeling for natural and treated water that contains particles. The goal of this study was to investigate the effects of particles on the transmission, measurement, and modeling of UV irradiation through aqueous media, relating to the UV disinfection process. Specific objectives were to (1) derive UV extinction and absorbance coefficients of scattering particles, semiscattering particles, and absorbing media; (2) compare the scattering albedo of alumina, clay, and natural particles from water and wastewater sources; (3) evaluate the effect of scattering particles on fluence rate distribution in a model UV reactor; and (4) compare the fluence rate distribution obtained experimentally to a mathematical fluence rate model. This study has implications for measurement of fluence distribution in UV reactors treating turbid water during disinfection of water and wastewater and UV light penetration in water columns under natural conditions such as drought or precipitation when concentrations of natural organic matter and particles vary.

2. Absorbance Measurements

A. Theory

Various studies on UV absorbance of water related to UV disinfection included the effect of particles on absorbance.[1–4] For full-scale UV system validation testing, solution transmittance is typically varied by spiking absorbing fluids such as coffee and humics into reactor feedwater[5,6]; however, these testing methods typically assume solutions devoid of particles. The standard method used to measure absorption relies on transmittance of light captured by a detector that is placed in line with the sample, using a spectrophotometer. The drawback of using this method is that particles that scatter light at angles outside the reception angle of the detector[4,7] (as shown in Fig. 1A) will result in significant error in absorbance measurements[8,9] or in UV fluence.[3,10,11]

H. Mamane (hadasmg@post.tau.ac.il) is with the Porter School of Environment, School of Mechanical Engineering, Tel-Aviv University, Tel-Aviv 69978, Israel. J. J. Ducoste is with the Department of Civil Construction and Environmental Engineering, North Carolina State University, Raleigh, North Carolina 27695. K. G. Linden (kglinden@duke.edu) is with the Department of Civil and Environmental Engineering, Duke University, Durham, North Carolina 27708-0287.
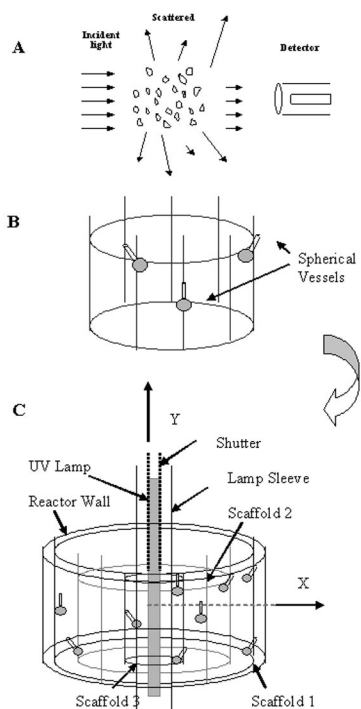
Fig. 1. A, Effect of particles on light scattering in all directions; B, one of the three scaffolds with three spherical quartz vessels attached to the scaffold; C, reactor with UV lamp (including shutter and sleeve) and three scaffolds inserted in the reactor (scaffold 1, 2, and 3) with spherical vessels attached to each scaffold.

True UV absorbance can be measured using integrating sphere (IS) spectrophotometers, optical devices that integrate the radiant flux of the most reflected and transmitted radiation simultaneously.[3,9–13]

Each particle scatters light in unique directions and patterns. As a result, the mutual influence of scattering from particles can lead to enhancement or cancellation of the integrated scattering effect. Scattering is influenced by the particle size, shape, chemical composition, and concentration.[14] For example, large-diameter particles such as 5 μm are dominated by forward scattering, whereas with small-diameter particles (i.e., 0.05 μm) the scattering is equally distributed in all directions.[15]

B. Methods

Conventional absorbance measurements, termed direct, were performed with a UV–visible dual-beam spectrophotometer (Varian, Model Cary 100BIO, Victoria, Australia) without the IS attachment in place. True absorbance measurements accounting for scattering by particles, were performed with the same spectrophotometer equipped with a 150 mm diameter IS attachment [Labsphere diffuse reflectance accessory (DRA-CA-30)] and a center mount sample holder used to position the sample inside the IS. The turbid sample is placed in a 1 cm path-length quartz cuvette with all four windows optically polished. The cuvette is fixed to a spring-loaded holder that hangs in the center of the sphere, connected to the top sphere cover.

C. Bench-Scale Testing

Bench-scale testing of scattering suspensions were conducted by direct and IS absorbance measurements, from 200 to 400 nm at 1 nm intervals, with the baseline adjusted with de-ionized (DI) water. A sample in which particles and absorbing media exist together is defined as a heterogeneous sample, whereas a sample devoid of particles is defined as a homogeneous sample. The absorbance coefficient (α) of a homogeneous sample is obtained by direct absorbance measurements[1] as follows:

$$\alpha(\text{cm}^{-1}) = \frac{A_D \ln(10)}{l} = \frac{A_D \, 2.303}{l}, \qquad (1)$$

where A_D is the direct absorbance measured by a conventional spectrophotometer and l is the path length of the cuvette that is equal to 1 cm (in this case) (detailed derivation is given in Ref. 3). The extinction coefficient is defined as the sum of the absorbance and scattering effects, as obtained by conventional spectrophotometric measurements of heterogeneous samples.[1] When the absorbance is measured by D for a heterogeneous sample, A_D, Eq. (1) will result in the extinction coefficient (β):

$$\beta(\text{cm}^{-1}) = \frac{A_D \ln(10)}{l} = \frac{A_D \, 2.303}{l}. \qquad (2)$$

The absorbance coefficient is the extinction coefficient corrected for light scattering.[16] The absorbance coefficient (μ) of a heterogeneous sample is obtained by IS absorbance measurements, A_{IS}, as follows:

$$\mu(\text{cm}^{-1}) = \frac{A_{\text{IS}} \ln(10)}{l} = \frac{A_{\text{IS}} \ln(10)}{l}. \qquad (3)$$

The scattering albedo, the fraction of light scattered away, is defined in percentage as

$$\omega(\%) = \frac{(\beta - \mu)}{\beta} \times 100. \qquad (4)$$

D. Calculated Path Length

The absorbance (unitless) is proportional to the concentration of absorbing components (c) and therefore

$$A = \varepsilon l c, \qquad (5)$$

where ε is the molar absorption coefficient in units of liters mol^{-1} cm^{-1}; however, here ε was modified and taken on a mass basis as liters mg^{-1} cm^{-1}. The true photon path length for a 1 cm cell (l) is derived by dividing the absorbance as measured by direct (A_D) for homogeneous samples or by IS spectroscopy (A_{IS}) for heterogeneous samples by the concentration (c) of the humic acid in milligrams per liter (mg/L) and the mass-based coefficient of the absorbing media (ε). For heterogeneous samples, using Eq. (6) will yield the

apparent path length, whereas using Eq. (7) will yield the true path length.

$$l = \frac{A_D}{\varepsilon c}, \tag{6}$$

$$l = \frac{A_{IS}}{\varepsilon c}. \tag{7}$$

3. Fluence Rate Measurements

A. Theory

UV disinfection systems often utilize low-pressure mercury lamps that emit monochromatic radiation at 254 nm. Although a common method of irradiance measurement on the bench scale is with a radiometer, use of a radiometer is not suitable for measuring the irradiation in an UV reactor, from an array of UV sources, nor with scattering suspensions because the radiometer measures irradiation normal to the planar surface of the detector.[17] Proper fluence rate measurement—the total radiant power from all directions onto an infinitesimally small sphere—can be approximated using an experimental tool that receives UV photons from different directions.[17,18] One extensively used alternative to traditional radiometry is chemical actinometry, such as the iodide–iodate process based on a photochemical reaction sensitive to 254 nm.[19,20] A spherical quartz vessel containing a chemical actinometer can measure UV fluence in air or in aqueous systems by placing the actinometer solution inside the sphere, placing the sphere in the UV-irradiated suspension, and measuring the photochemical reaction occurring inside the sphere.[6,17,21] In this study we hypothesized that spherical actinometry is the best approach to quantify UV fluence with scattering suspensions.

B. Methods for Actinometry Preparation

The iodide–iodate actinometer is based on the following photochemical reaction[20]:

$$8\ I^- + IO_3^- + 3\ H_2O + h\nu \rightarrow 3\ I_3^- + 6\ OH^-. \tag{8}$$
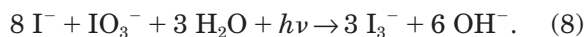
The solution at first is optically transparent above 330 nm; however, upon exposure to UV irradiation at 254 nm the photoproduct tri-iodide ion (I_3^-) that is formed exhibits a strong absorption at $\lambda = 352$ nm with a molar absorption coefficient of $\varepsilon_{352} = 27{,}636$ M^{-1} cm^{-1} in a 0.6 M KI/0.1 M KIO_3 solution.[6] The quantum yield of this actinometer (Φ) was taken as 0.64 at 254 nm and 20.7 °C. The KI/KIO_3 actinometry stock solution was prepared according to Ref. 20 and was made fresh daily. Values of the blank actinometer prior to UV exposure (i.e., the unirradiated control) were taken as A_{352} (blank). After UV exposure the actinometer was immediately transferred to a quartz cuvette with a 1 cm path length, and absorbance was measured at 352 nm and labeled A_{352} (sample). The ideal exposure time (seconds) of the actinometer inside the sphere was found experi-

Table 1. Coordinates of Spherical Actinometer Positions in the Annular Ultraviolet Reactor

Scaffold Number	Vessel Number	X (cm)	Y (cm)
1	1	10.55	4.6
1	3	9.55	−7.7
1	5	−11.15	0.9
2	7	7.35	4.2
2	9	6.95	−8.3
2	11	−7.45	−0.1
3	13	3.75	4.7
3	15	4.05	−8.4
3	17	−4.35	−0.7

mentally to avoid saturation of the actinometer. Repetitions were conducted to achieve statistical precision (i.e., a low standard deviation). The fluence rate (E') was calculated by

$$E' = \frac{[A_{352}\ (\text{sample}) - A_{352}\ (\text{blank})]\ V\ (\text{mL})}{\text{area}\ (\text{cm}^2)\ \text{exposure time (s)}\ \phi\varepsilon_{352}}$$
$$\times\ U\ (\text{mW cm}^{-2}), \tag{9}$$

where U is the constant used to convert einsteins into conventional UV fluence units of millijoules at 254 nm wavelength (4.72×10^8 mJ einstein^{-1}).

C. Ultraviolet Reactor Testing

Fluence rate distribution in an annular batch UV reactor was obtained by the spherical actinometry method. Spherical actinometry is a technique whereby an actinometer is placed inside a quartz vessel, which can then record photons coming from all directions. The spherical quartz vessels are approximately 1 cm in diameter, with a volume of 0.4–0.5 mL and a cross-sectional area (an area that intercepts the radiant energy) of 0.65–0.77 cm^2. Spheres are composed of the sphere vessel that holds the liquid and a narrow extending stem through which the liquid is filled into or withdrawn out of the sphere and that also serves as a holding location.

As described in Fig. 1C and previous studies,[22,23] a low-pressure lamp (16 W, Ster-L-Ray, Atlantic Ultraviolet, Haupauge, New York) surrounded by a 3.7 cm quartz sleeve was placed vertically in an annular bench-scale UV reactor. The reactor dimension was 17.8 cm in height and 24.5 cm in diameter, with a total volume of 8.2 L. Three metal scaffolds identified as 1, 2, and 3 with radial diameters of 23, 16, and 10 cm, respectively, were placed in the reactor, with spherical vessels attached at various fixed radial and longitudinal (X, Y) positions from the center of the lamp (Figs. 1B and 1C and Table 1). The scaffolds and the spheres were placed in the reactor in a manner that avoided shadowing from the other inner scaffolds. A manual shutter between the UV lamp and the quartz sleeve was used to adjust the UV exposure level. Prior to each exposure, the lamp was warmed

Table 2. Analytical Measurements of Total Suspended Solids, Dissolved Organic Matter, Mean Diameter, Percent Volatile Solids (% VSS/TSS), Turbidity, and Particle Counts

Particle Type	TSS (mg/L)	DOC (mg/L as C)	Mean Diameter (μm)	% VSS/ TSS	Turbidity NTU	Count (per mL)
No particles	0	0.18, 0.36, 0.74	—	—	—	—
Alumina	95	0, 0.18, 0.36, 0.74	$D_{50}{}^a = 0.4$	—	310	—
Alumina	190	0, 0.18, 0.36, 0.74	$D_{50} = 0.4$	—	680	—
Alumina	380	0, 0.18, 0.36, 0.74	$D_{50} = 0.4$	—	1445	—
Clay	190	0, 0.36, 0.74	1	—	315	1.5×10^8
WW$_{EFF}$[b]	280	22	3.7	17.6	2.3	4.9×10^4
WW$_{AUG}$[c]	293	22	3.5	21.7	6.3	2.1×10^5
WW$_{AUG}$	328	22	5.5	22.6	17.5	1.9×10^5
WW$_{AUG}$	374	22	5.6	33.4	33.4	3.1×10^5
SW[d]	84	11.1	1.3	22.4	4.5	1.5×10^6
SW$_{PD}$[e]	91	3.97	1.2	25	0.1	2.9×10^4

[a]D_{50} for alumina from manufacturer; alumina count per milliliter is not possible as the average size diameter is below the sensitivity of the particle size analyzer.
[b]Wastewater effluent.
[c]Wastewater effluent samples augmented with MLSS particles.
[d]Surface water.
[e]Sampled surface water collected after filtration prior to disinfection.

up to a constant irradiance. After exposure, the solution or suspension with particles was drained out of the reactor, the scaffolds were removed, and the actinometer was withdrawn from the spheres by a Pasteur pipet. The actinometer was transferred to 1 cm cuvettes for absorbance measurements of the photoproduct at each X, Y location tested. Three spheres were attached to each of the three scaffolds to provide a total of nine locational measurements for each condition tested.

4. Particles and Analytical Methods

A. Particles Used in Bench-Scale and Ultraviolet Reactor Systems

1. Clay Particle Preparation
The clay type used was SWy-2, which is Na-rich montmorillonite (Crook County, Wyoming) obtained from the Clay Minerals Society (Source Clays Repository). Clay particles were suspended in DI water at a concentration of ~1 g/100 mL and placed in 100 mL graduated cylinders to allow the coarse particles to settle for three days. The supernatant collected was used in the experiments.

2. Alumina Particle Preparation
Submicrometer alumina particles (aluminum oxide, Al_2O_3) of type CR 15 (Baikowski International Corp., Charlotte, North Carolina) were used, with d_{50} of 400 nm, as obtained by the manufacturer datasheet. Alumina particles were suspended in DI water with a dispersant (Darvan 821, Vanderbilt Co., Norwalk, Connecticut) to form a well-dispersed suspension at 0.1 wt. % of the dry alumina. The dispersant was initially added to DI water, sonicated (Branson 1200, Branson Ultrasonics Corp., Danbury, Connecticut), and subsequently the alumina was added while sonicating for an additional 5 min.

3. Humic Acid Preparation
Leonardite humic acid was obtained from the Gascoyne Mine in Bowman County, North Dakota, and isolated by the International Humic Substances Society. A stock solution was prepared by dissolving 1 g/L in 1 M NaOH. The solution was then acidified to neutral pH and filtered through a 0.22 μm nylon membrane filter (Millipore, Bedford, Massachusetts).

4. Natural Water and Wastewater Samples
Natural raw water was collected from the Williams Water Treatment Plant in Durham, North Carolina, and wastewater samples were collected from the North Durham Water Reclamation Facility, Durham, North Carolina.

B. Analytical Methods
Particle mean diameter, particle size distribution, and particle concentration measured as counts per milliliter (μm/mL) were obtained with a Multisizer 3 (Beckman Coulter, Inc., Miami, Florida). Turbidity was measured by a turbidimeter (Hach, Model 2100N, Loveland, Colorado). Total suspended solids (TSS) and volatile suspended solids (VSS) were measured according to the Standard Methods for the Examination of Water and Wastewater (Ref. 24, Method 2540B and 2540E, respectively). Total organic carbon (TOC) was measured by a TOC analyzer (Tekmar-Dohrmann, Apollo 9000, Cincinnati, Ohio), and dissolved organic carbon (DOC) measurements were conducted by filtering a solution through a 0.45 μm glass fiber filter (Millipore, Bedford, Massachusetts) before utilizing the TOC analyzer. Table 2 presents a summary of these parameters. Scanning electron microscopy (SEM) images of particles were performed with a Philips XL30 environmental scanning electron microscope (FEI Company, Hillsborough, Oregon).

C. Conditions Tested

Seven different conditions were tested to evaluate the effect of particle suspensions on absorbance and scattering in a bench-scale system (Subsection 2.C) and on fluence distribution in a UV reactor (Subsection 3.C):

1. Highly scattering and low absorbing particles: suspension of alumina particles suspended in DI water.

2. Highly UV absorbing media: a solution of humic acid devoid of particles.

3. Highly UV absorbing media mixed with highly scattering particles: a suspension of alumina particles in water spiked with humic acid.

4. Partially scattering particles: a suspension of clay particles suspended in DI water.

5. Highly UV absorbing media mixed with partially scattering particles: a suspension of clay particles in water spiked with humic acid.

6. Natural particles: surface water from reservoir of water treatment plant (SW); surface water after coagulation, filtration, and prior to disinfection (SW_{PD}); and surface water filtered in the laboratory with 0.2 μm filter (SW_{FIL}).

7. Natural particles: wastewater effluent (WW_{EFF}) and wastewater effluent after augmenting with mixed liquor suspended solids (MLSS) (WW_{AUG}).

5. Radiative Transfer Equation

Although researchers have developed alternative approaches to modeling UV light in a participating medium (i.e., a medium that reflects, refracts, absorbs, and scatters light),[23] only the radiative transfer equation (RTE) accounts for all these physical properties. Researchers have been successful in using the RTE to predict the fluence rate distribution in a participating medium that includes these physical properties.[1,25,26] However, the inclusion of light-scattering effects imposes an additional level of uncertainty due to the scattering phase function.[25] The scattering phase function can be based on analytical functions, albeit, under specific conditions (i.e., particle type, size, and concentration).[25] Consequently, accurate determination of the appropriate scattering phase function for the specific participating medium continues to be a challenge and is a likely source of error if sufficient experimental fluence rate data are not available.

The RTE [Eq. (10)] was used to simulate the fluence rate in this study. The RTE accounts for absorption and scattering effects when heat passes through a homogeneous and isotropic medium:

$$(\Omega\nabla)\underset{I}{I(r,\ \Omega)} = -\underset{II}{\left(k_a + k_s\right)}\underset{III}{I(r,\ \Omega)} + \underset{IV}{k_a I_b(r)}$$
$$+ \frac{k_s}{4\pi} \underset{\Omega=4\pi}{\int} I(r,\ \Omega')\phi(\Omega'\rightarrow\Omega)\mathrm{d}\Omega',$$
$$\underset{V}{} \qquad (10)$$

where Ω is the direction of propagation of the radiation beam; k_a, k_s are the absorbance and scattering coefficients (1/m) [that correlate to μ and (β − μ) in SI units]; I_b is the intensity of blackbody radiation; and ϕ is the scattering phase function.

As shown in Eq. (10), part I of the RTE is the gradient of intensity along the propagation direction, part II is the loss due to absorption, part III is the loss due to outscattering, part IV is the gain due to blackbody emission, and part V is the gain due to inscattering. Although Eq. (10) was originally proposed for the heat transfer in one medium, several researchers[27,28] have improved it to model radiative transfer in the multilayer medium with Fresnel interfaces (i.e., refraction effects). Simulations were performed with and without refraction to investigate the influence of refraction on the RTE results. In addition, the fluid media were considered cool and therefore term IV was neglected. In this study, a commercially available software, known as FLUENT (Lebanon, New Hampshire), which has a built-in version of the discrete ordinate approach to solve the RTE, was used to predict the fluence rate distribution inside the test reactor. For tests conducted with particles, scattering was assumed to be isotropic (i.e., uniform over the particle surface).

In the discrete ordinate approach, angular discretization around the lamp periphery was required to define the direction of the light ray path where Eq. (10) was solved. In this study, the lamp periphery was divided into four divisions both in the theta and phi directions. Finer angular discretization was tested but showed no significant improvement. The lamp boundary condition (429 W/m²) was defined by taking the fraction of the lamp power at 254 nm within the reactor (3.6 W) and dividing by the surface area of the lamp within the reactor (8.39×10^{-3} m²). A diffuse wall boundary condition was used to describe the incident radiation from the reactor surface. Numerical convergence was based on two requirements. First, the sum of the absolute residual radiant source over the whole solution domain must be less than 0.001% based on the total radiant power. Second, the values of the monitored irradiance at several locations must not change by more than 0.001% between successive iterations. Monitor locations include near wall regions, near the lamp surface, and the main tank region. The different regions were monitored for several iterations to determine whether the convergence criterion was met. The overall grid size was determined through successive refinement in the grid until changes in the irradiation intensity profiles were less than 0.01% between successive refinements.

6. Results and Discussion

A. Effect of Particle Characteristics on Absorbance

Figure 2 illustrates images of alumina, clay, surface water, and wastewater effluent, particles obtained by SEM. Surface water and wastewater effluent particles varied in size and shape, whereas primary alu-
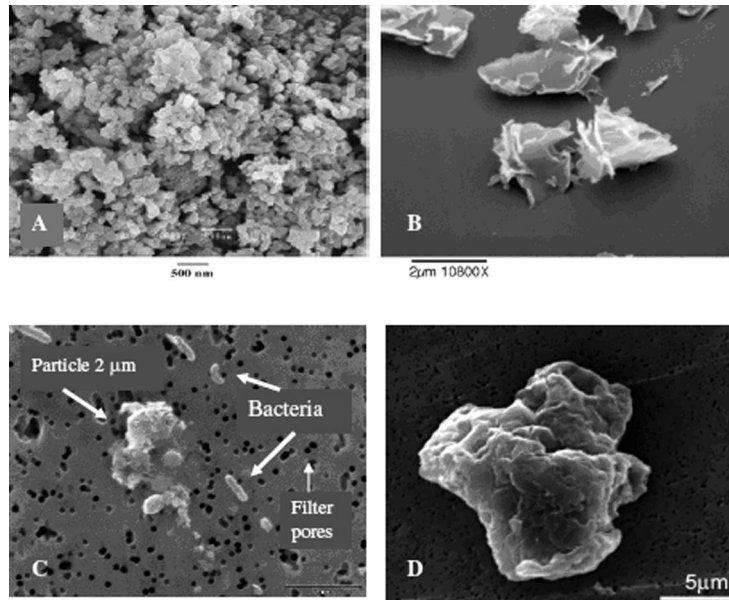
Fig. 2. SEM images of particles used in this experiment: A, images of alumina particles; B, clay; C, surface water; D, wastewater effluent. (Image A of alumina particles are type CR 15 from Baikowski International Corp., Charlotte, North Carolina).

mina and clay particles were less variable in size and shape, when excluding aggregates. Other particle characteristics such as mean diameter; turbidity; suspended solids; percent volatile solids; DOC; and particle count of clay, alumina, surface water, and wastewater effluent are described in Table 2. Aluminum is highly reflective at all visible wavelengths and into the far UV, making it commonly used for coating of mirrors,[14] and was used to simulate submicrometer particles with high scattering ability. Montmorillonite clay particles were chosen as representative of natural inorganic particles in water[29] at the micrometer size range of typical colloids in water treatment plants. Surface water and wastewater effluent were evaluated due to the practical implications for UV disinfection of waters in a treatment plant. Particle concentration, diameter, wavelength of light, refractive index of particles relative to the medium, and shape if the particle is nonspherical all affect the intensity of scattered light.[14,15] Consequently, variability in size, shape, and chemical composition of particles were used in this study to assess the scattering pattern.

As a light beam passes through a solution it will become attenuated by absorbing substances and by reflection from particles.[18] Nonabsorbed light including the scattered light and the transmitted light is measured with an IS.[4] With the IS, light that exits the sample inside the cuvette at any angle is reflected by the highly reflecting sphere and measured by the detector mounted on the sphere wall. Performance of the IS was validated by a suspension with high absorption and no scattering and by a suspension with high scattering and low absorption. In Fig. 3, the UV absorbance, as measured by direct and IS spectroscopy, is plotted as a function of alumina concentration for samples with or without humic matter at concen-

trations of 0, 6, and 12 mg/L TOC. As the concentrations of the alumina particles increase from 12.5 to 250 mg/L for a fixed humic concentration, the associated UV absorbance as measured by IS remains constant [samples IS (0 mg/L), IS_H (6 mg/l), and IS_H (12 mg/L)]. As the concentrations of the particles increase, the associated UV absorbance as measured by direct measurement increases linearly, with a difference in intercept that correlates to humic acid concentration [samples D (0 mg/L), D_H (6 mg/L), and D_H (12 mg/L)]. The difference in average slope for different humic concentrations derived from the linear correlation between absorbance and particle concentration was not significant, indicating that the effect of scattering on absorbance as measured by the direct method is independent of the humic con-
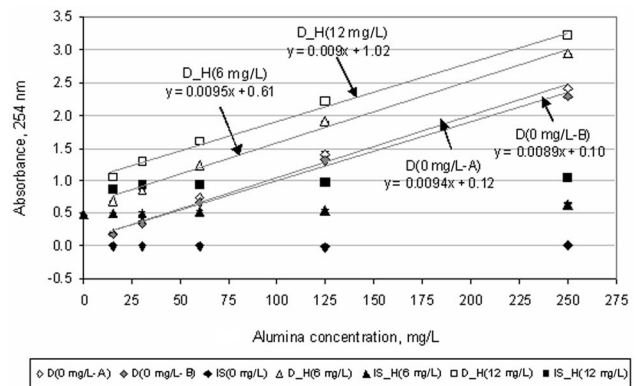

Fig. 3. Effect of varying suspended alumina particle concentration on direct (D) and IS absorbance measurements, with or without fixed humic acid concentration. H represents humic acid and the label values in parentheses represent the concentration of humic acid. Absorbance was measured in 1 cm cuvettes.
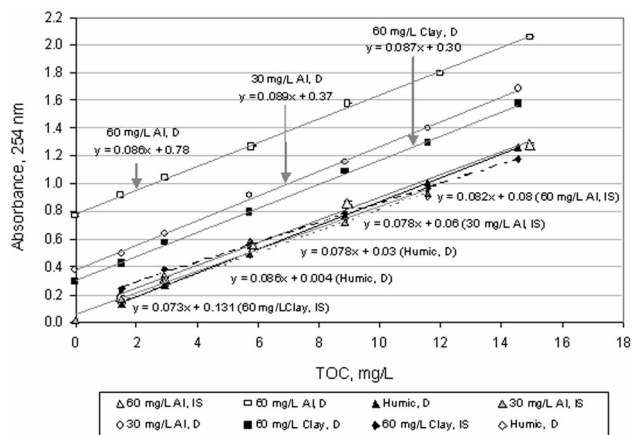
Fig. 4. Effect of varying humic acid concentration, measured in milligrams per liter TOC, on direct (D) and IS absorbance measurements of fixed concentration of suspended alumina and clay particles. Al represents alumina particles.
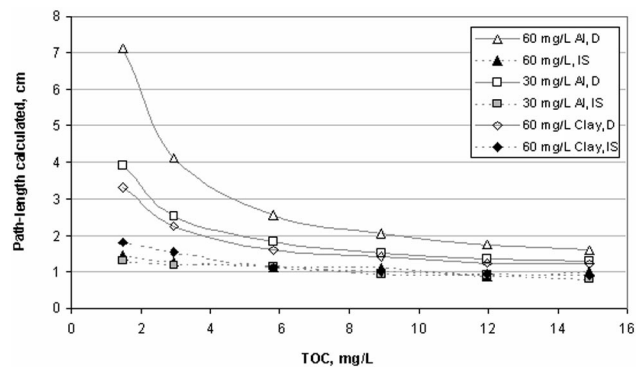

Fig. 5. Effect of varying humic acid concentration, measured in milligrams per liter TOC, on calculated light path length for a fixed concentration of suspended alumina (Al) and clay particles.

centration. The intercept was dependent on humic concentration and increased at ~0.5–0.6 mW/cm^2 absorbance units over a 1 cm path length for each addition of 6 mg/L TOC.

In Fig. 4, the UV absorbance as measured by the direct and IS spectroscopy is plotted as a function of humic concentration from 0 to 15 mg/L TOC for samples with or without alumina or clay particles at concentrations of 0, 30, and 60 mg/L to assess scattering trends. As the concentration of humics increases, the UV absorbance as measured by IS for samples with particles or as measured by direct spectroscopy for samples devoid of particles falls approximately on the same slope. As the concentration of humic acid increases for a fixed alumina or clay concentration, the absorbance measured by the direct spectroscopy increases linearly with similar slopes over the different particle suspensions—however, with different intercepts that correlate to the particle type (clay or alumina) and concentration (30 or 60 mg/L). These findings (Figs. 3 and 4) provide evidence that the influence of particle scattering is correctly measured using the IS technique for fluence determination of scattering particles. More importantly, these results clearly point out the drawbacks of using the direct conventional spectrophotometer with samples containing particles.

The percent difference between absorbance values as measured by direct spectroscopy (A_D) compared with absorbance values as measured by IS spectroscopy (A_{IS}) was calculated for each case by the following equation:

$$\mathrm{diff}(\%) = \frac{A_D - A_{IS}}{A_{IS}} \times 100. \quad (11)$$

Using the particle concentrations described in Table 2, the direct method overestimated the absorbance at 254 nm by 110%–140% for homogeneous and heterogeneous clay particles and by 25% for

wastewater effluents. Particles from the MLSS augmented to wastewater effluent increased the percent difference to 50%–65% (from 25%), indicating that an increase in TSS of 100 mg/L resulted in up to a threefold increase in absorbance overestimation. The difference between $A_D - A_{IS}$ for a suspension of alumina and humics is fixed at any humic concentration, whereas the percent difference increased linearly with alumina concentration and was higher for the sample with lower humic concentration. The difference between $A_D - A_{IS}$ of water after filtration and prior to disinfection is smaller compared with raw water; however, dividing by a smaller value of A_{IS} resulted again in a larger percent difference. Therefore high percent differences provide an assessment of the overestimation in absorbance values that in general increase with particle scattering—however, not when absorbance values are very low. Low absorbance values in the denominator will result in enormous values that do not necessarily reflect scattering but may reflect the low sensitivity in measuring low absorbance. The tolerance in absorbance of one absorbance unit with a conventional spectrophotometer as described in Subsection 2.B is ±0.0050.

B. Effect of Scattering on Photon Path Length

Figure 5 illustrates the effect of varying humic acid concentration, measured in milligrams per liter TOC, on the photon path length for a given suspension of alumina or clay particles. In a highly scattering solution, it is possible that each photon takes longer than a 1 cm path within a 1 cm cuvette. The path length (l) of light was calculated according to Eqs. (6) and (7), with a mass basis absorption coefficient (α) of 0.086 L mg^{-1} cm^{-1}, which is the humic acid absorbance average slope as a function of humic concentration (Fig. 4). Using IS spectroscopy, the light path length in a 1 cm cuvette with a heterogeneous alumina scattering suspension matched the actual path length of 1 cm. Using IS spectroscopy for clay particles at low TOC values of 1–3 mg/L resulted in a light path length that deviated from the actual path length of 1 cm. The path length of clay suspensions does truly increase (l equals 2 cm, TOC of 1 mg/L), but the
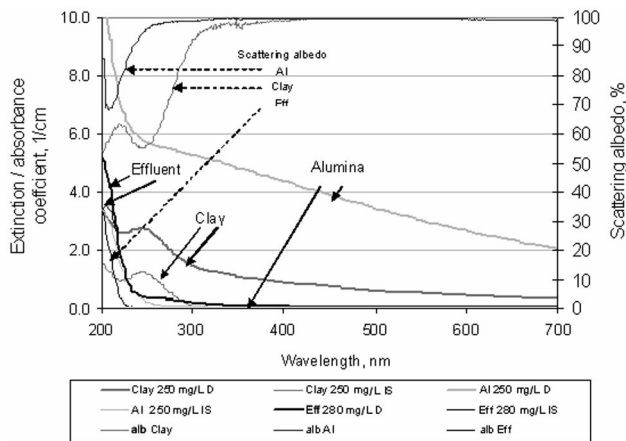
Fig. 6. Direct (D) and IS spectral absorbance measurements and scattering albedo of alumina (Al), clay, and wastewater effluent suspensions at 280 mg/L.

Table 3. Summary of Extinction Coefficient, Absorbance Coefficient, and Scattering Albedo for Various Conditions Tested in the Annular Ultraviolet Reactor

Sample	Extinction Coefficient (1/cm)	Absorbance Coefficient (1/cm)	Scattering Albedo (%)
95 Al	2.45	0.01	99.39
190 Al	4.80	0.08	98.30
380 Al	9.15	0.08	99.17
95 Al + 0.18 H[a]	2.72	0.07	97.49
190 Al + 0.18 H	4.85	0.16	96.79
380 Al + 0.18 H	9.21	0.16	98.26
95 Al + 0.36 H	2.49	0.12	95.38
190 Al + 0.36 H	4.85	0.17	96.43
380 Al + 0.74 H	9.19	0.21	97.70
95 Al + 0.74 H	2.54	0.23	91.03
190 Al + 0.74 H	4.92	0.30	93.93
380 Al + 0.74 H	9.17	0.29	96.85
190 Cl[b]	1.728	0.816	52.81
190 Cl + 0.36 H	1.761	0.801	54.50
190 Cl + 0.74	1.803	0.915	49.25
WW$_{EFF}$ 280	0.18	0.14	20.49
WW$_{AUG}$ 293	0.20	0.13	36.78
WW$_{AUG}$ 328	0.29	0.19	32.36
WW$_{AUG}$ 374	0.42	0.25	39.39
SW	0.79	0.64	18.94
SW$_{PD}$[c]	0.14	0.06	56.61

[a]H, humic acid.
[b]Cl, Clay.
[c]At low particle absorbance the scattering albedo is inaccurate.

amount of increase is measured (falsely) higher with direct measurement (l equals 3.3 cm, TOC of 1 mg/L).

The path length of light as calculated using the direct measurement at 1 mg/L TOC increased severalfold and depended on the particle type and concentration. This increase is a result of loss of light due to scattering and not the actual path length the light travels. For similar particle concentration (60 mg/L direct alumina versus clay), the apparent path length a photon travels until exiting the cuvette is larger for alumina due to its increased scattering and lower absorbing properties. As the absorbance of humics increase, the photon's path length is shortened because it is extinguished by the absorbing media before it travels along its path. Amplified path-length results from multiple scattering,[7] which is likely caused by the increased apparent path length in direct absorbance measurements. Highly scattering nonabsorbing alumina particles can be used as a method to validate true path length with IS spectroscopy. Clay particles are not suitable for validation as they absorb part of the UV light.

C. Extinction and Absorbance Coefficients and Scattering Albedo

Figure 6 illustrates the direct and IS spectral extinction and absorbance coefficient and scattering albedo of alumina, clay, and wastewater effluent suspensions as a function of wavelength. It is evident that the particle chemical makeup affects the light-scattering patterns, with a general decrease in extinction and absorbance coefficient with increase in wavelength. Inorganic alumina and clay particles scatter light at all wavelengths including visible light; however, wastewater effluents do not. Natural water typically absorbs UV in the lower wavelengths (200–240 nm); therefore these wavelengths may not be available for UV disinfection.[30] Light extinction dominated by scattering is nearly independent of photon energy for particles larger than the wavelength of light.[14] Interestingly, the scattering albedo

of alumina particles, with an average diameter of 400 nm, appears to be nonsloping above 400 nm. Medium-pressure lamps used for disinfection of water and effluents emit light at wavelengths over a wide spectrum in the UVC and UVB ranges. The spectral scattering characteristic of particles across these wavelengths emphasizes the complexity unique to medium-pressure lamps for UV disinfection of micro-organisms cosuspended with scattering particles in wastewater effluents.

Table 3 summarizes the extinction coefficient, absorbance coefficient, and scattering albedo for various conditions tested in the annular UVC reactor. Particles from wastewater effluent exhibit a lower scattering albedo at 254 nm (approximately 20%–40% scattering) compared with inorganic alumina (90%–100% scattering) and Na-montmorillonite clay particles (50% scattering). As an example, TiO_2 has a scattering albedo of 56% at 355 nm; however, most materials have a lower albedo than TiO_2.[4] In comparison, the scattering albedo is ~100% for alumina and clay particles above approximately 300 nm, whereas the scattering albedo is 0% for wastewater effluent at those wavelengths (Fig. 6). The IS absorbance of alumina particles is practically zero indicating that the scattering light was completely captured by the detector.

High levels of scattering in aquatic particles are typical for samples consisting of inorganic mineral detritus particles.[7] The inorganic portion of natural
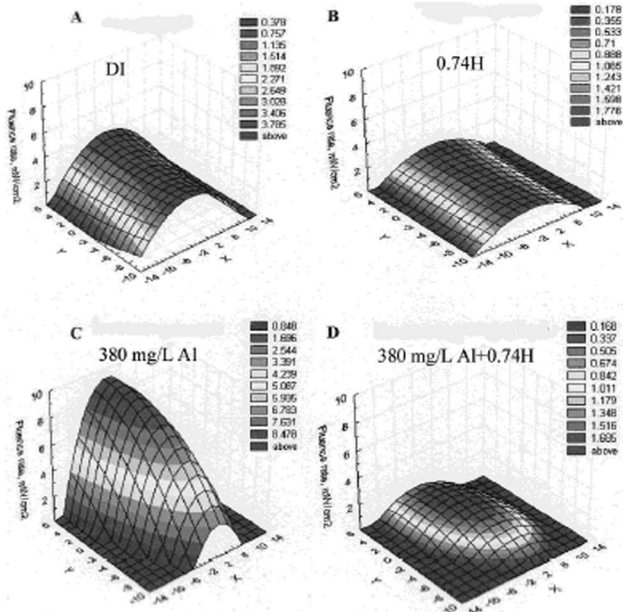
Fig. 7. Three-dimensional surface plots of fluence rate distribution in the annular UV reactor at various X, Y locations for conditions of A, DI water; B, 0.74 mg/L TOC solution (0.74 H); C, concentration of alumina particles (380 mg/L Al); D, combination of particle and humic (H) (380 mg/L + 0.74 H). Interpolation in the figure is based on a nine-point grid.
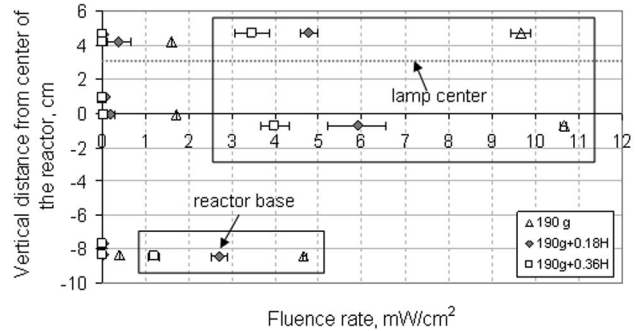

Fig. 8. Measured actinometry fluence rate at vertical distances from the center of the reactor for each sphere in the case of a fixed alumina suspension of 190 mg/L with varying humic (H) concentration. Data in boxes are the fluence rate values obtained for scaffold 3, situated closest to the lamp, for the various conditions in the legend.

particles can be described by the ratio of volatile-to-suspended solids subtracted from unity (Table 2). Approximately 91%–98% of wastewater effluent (WW_{EFF}) and effluent augmented with particles (WW_{AUG}) is comprised of inorganic material, compared with 75%–78% for surface water (SW) and treated filtered water (SW_{PD}). The larger percent of the inorganic portion in natural water seems to relate to the larger scattering albedo of inorganic particles. The correlation between water quality and scattering ability of natural water and wastewater effluents may be of interest for future studies.

D. Fluence Rate Distribution Measured by the Spherical Actinometry for Reactor-Scale Experiments

Figure 7 illustrates the three-dimensional surface plots of fluence rate in the annular UVC reactor based on nine X,Y points (three for each scaffold) for certain conditions, where X and Y are radial and vertical distances from the center of the lamp (Table 1). As expected, in all tests, the fluence rate peaks near the center of the lamp and decreases with increasing X (i.e., radial) distance from the lamp ($X = 0$ to $X \cong \pm 11$ cm). Note that, due to physical constraints of the reactor setup, the actual center point of the lamp is located 2.9 cm above the center of the reactor, which results in a slight shift in the peak intensity toward $Y = 2.9$ cm. Exposure times in the annular reactor were kept short, to between 5 and 20 s, during which the particles did not settle.

The peak fluence rate measured near the center of the lamp ($X = 0$) was used to compare the different conditions in Fig. 7. Adding 0.74 mg/L humic acid (absorbance of humic at 254 nm, $l = 1$ cm is 0.067) reduced the peak fluence rate from 3.8 mW/cm^2 with DI water to 1.7 mW/cm^2. On the other hand, adding 380 mg/L alumina particles to DI water increased the peak fluence rate tremendously, from 3.8 with DI to 8.9 mW/cm^2. However, when 0.74 mg/L humic acid was added to the alumina suspension, the peak fluence rate reduced back down to 1.8 mW/cm^2, similar to the fluence rate of 0.74 mg/L humic in DI water.

Light intensity penetrates through a radial distance of ~ 11 cm with humic acid, which is close to the reactor wall, whereas the combination of alumina and humics, in this case, permits light to penetrate only up to a radial distance of 4 cm. At a radial distance of 7 cm ($X = 7$), humic acid reduces the fluence rate compared with DI water, whereas alumina particles increase the fluence rate, but to a value below that for DI water. Interestingly, the combination of humic and alumina reduces the fluence rate to zero and not to a fluence rate value between alumina and humic. Increased fluence rate with alumina particles is a result of multiple scattering and increased path length. In the presence of absorbing humic material, this multiple scattering is likely responsible for complete extinction of photons at 7 cm from the lamp, due to multiple passes across the absorbing humics.

The fluence rate for the vertical distance from the center of the reactor for 190 mg/L alumina suspension with varied humics is illustrated in Fig. 8. At vertical distance of ~ 8 cm below the reactor center (X varies, $Y \approx 8$), the spherical vessels are close to the base of the reactor. The spheres positioned at the reactor base receive lower fluence due to the following: (a) the reactor wall and base are acting as a partial sink for photons and (b) the region near the ends of the lamp emit slightly lower intensity light compared with the center of the lamp. Researchers have shown that a linear lamp can be approximated as a series of segment sources that produce light normal to the lamp surface and go down as the cosine
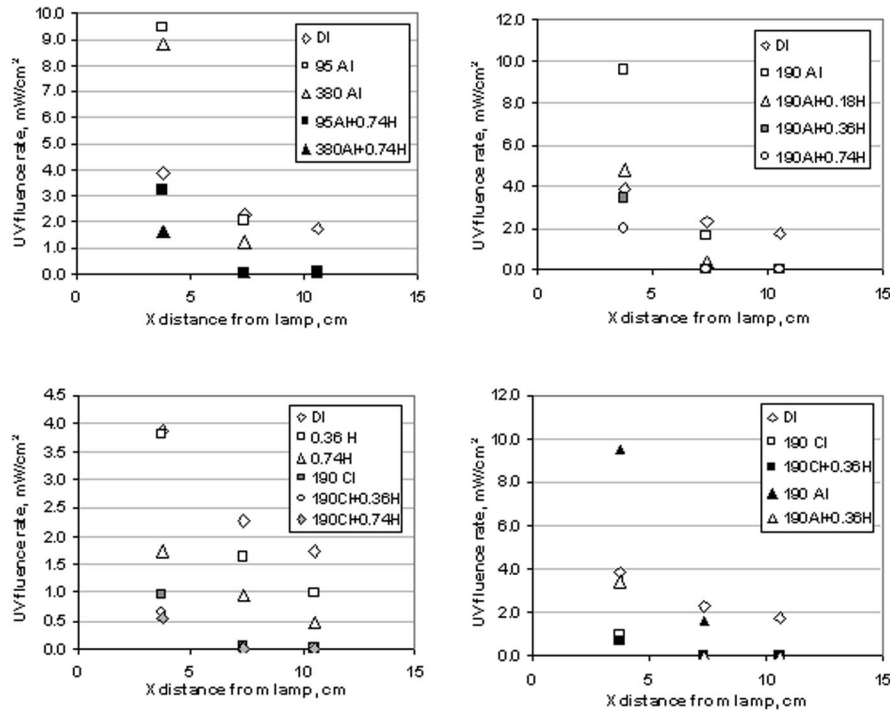
Fig. 9. Fluence rate distribution in the annular UV reactor for various conditions tested: A, varying Al and humic (H) concentrations; B, fixed Al and varying humic concentrations; C, fixed clay (Cl) with varying humic concentrations; D, similar concentration of alumina and clay particles.

of the angle between the surface normal and the direction vectors.[23] Consequently, the highest fluence rate will be found near the center of the lamp while the lowest will be found near the lamp ends. In Fig. 8 it is difficult to differentiate between the data points in the farthest scaffolds (1 and 2) because the fluence rate is between 0 and 0.5 for samples with humics added to the clay suspension. Data enclosed in the box in Fig. 8 are fluence rate values obtained for scaffold 3, which is the one closest to the lamp center. Within the box, increasing the concentration of humic acid resulted in lower penetration of UV light through the reactor for a fixed particle concentration.

The fluence rate distribution for a radial distance (X) with different alumina and clay conditions is illustrated in Fig. 9. For clarity, only the positive distances from the lamps are shown because the negative side is a mirror of the positive side. In all the graphs of Fig. 9, the fluence rate decreases with radial distance. Humics dissolved in DI water or suspended with alumina or clay particles reduced the fluence rate, with a more pronounced effect in the presence of alumina particles compared with clay particles, and with higher alumina concentration compared with lower concentration (Figs. 9A–9D). Alumina suspensions (without humics) increased the UVC fluence rate distribution up to 2.5-fold (Fig. 9B), whereas clay particles at similar particle concentration but different size, shape, and composition reduced the fluence rate distribution fourfold compared with DI water (Fig. 9D). Clearly the decrease in flu-

ence rate depends on the nature and concentration of the particle and the absorbing media.

The fluence rate distribution for a radial distance (X) of natural water samples tested is illustrated in Fig. 10. Untreated surface water turbidity with 4.5 nephelometric turbidity units (NTU) (SW4.5), after treatment in a water plant for coagulation and filtration (SW$_{PD}$), resulted in 0.1 NTU and a fourfold increase in fluence rate due to removal of both absorbing aqueous media and particulates (Fig. 10A). Consequently, coagulation and filtration does work to reduce organic matter and increase the transmission, which is beneficial for UV penetration and has implications for where to place UV technology in the water treatment process train. Separating out the effect of the absorbing components in the water from the scattering components of the particles is not possible as natural water and effluents are a mixture of inorganic and organic particles that absorb UV in addition to the dissolved aqueous matter. It is possible, however, to subtract the effect of the particles by filtering the sample. Surface water (SW7) partially filtered through a 0.2 μm filter and partially mixed with unfiltered SW7 water resulting in 1 NTU (SW$_{FIL}$l) exhibited a higher fluence rate due to removal of UV absorbing particles.

Water with 4.5 NTU (SW4.5) exhibited a similar fluence rate as water with 7 NTU (SW7), implying that in addition to turbidity, other parameters such as filtered TOC and absorption of a soluble portion of water and particles are all factors to consider in par-
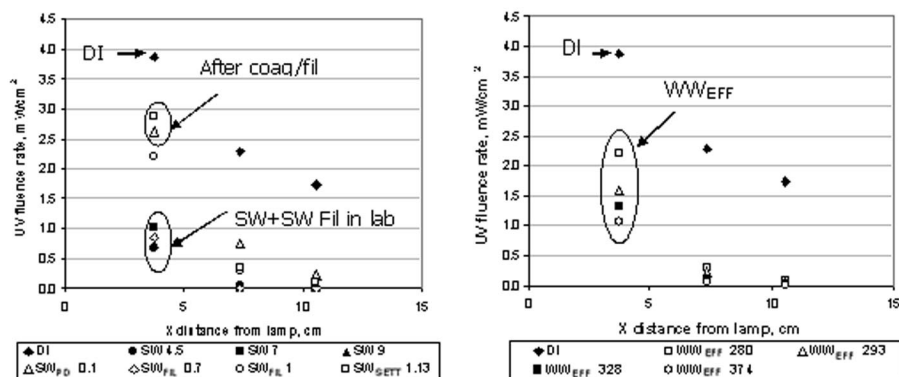
Fig. 10. Fluence rate distribution in the annular UV reactor for A, surface water and B, effluent augmented with MLSS particles. coag, cogulation; floc, flocculation; fil, filtration.

ticle effects. At low particle concentration, usually below 1 NTU as with drinking water, the intensity of scattered light is typically proportional to the particle concentration. This is in contrast to wastewater samples where multiple scattering is usually apparent above 5 NTU.[15]

The fluence rate of wastewater effluents augmented with MLSS (WW$_{AUG}$) decreased with an increase in particle concentration. This indicates that adding particles to a similar background solution increased absorbance of the total bulk solution and was the cause of the reduced germicidal UV (Fig. 10B), as previously suggested in Ref. 3. Correlation between water quality parameters (as TSS, percent VSS, mean particle diameter) to the absorbance coefficients and fluence rate were not clear, although some trends could be noted. Other researchers also could not find correlations between parameters as suspended solid concentration to scattering and absorbance of activated sludge effluents.[3]

E. Radiative Transfer Equation Model

Knowledge relating to extinction and absorbance coefficients can be used to solve the spatial distribution of intensity inside a reaction space using RTEs.[1] In general, equations that describe scattering coefficients depend on spectral absorption, outscattering, and inscattering.[1,31] However, equations of inscattering contributions are difficult to solve. Consequently, experimental measurements provide an alternative approach.[1] It is desired to minimize inscattering contributions and simultaneously minimize collection of outscattered radiation in the forward direction by the detector. Since inscattering cannot be isolated, it is important to obtain the extinction or absorption coefficient to solve the RTE[1] to understand how well a numerical model describes the fluence rate within a reactor that contains both absorbing and scattering properties.

Figure 11 displays the RTE model predictions compared with the experimental fluence rate results for the different conditions explored in this study. In Fig. 11A, the RTE model was used to predict a purely absorbing nonscattering medium. The RTE model

was found to reasonably predict the experimental measurements under these absorbing nonscattering conditions. In Fig. 11B, the RTE model was used to predict a purely scattering nonabsorbing medium and was found to predict the experimental conditions at the 190 and 380 mg/L particle concentration. However, at the 95 mg/L concentration, the model significantly overpredicted the experimental results. The overprediction at this low concentration suggests that there may be an additional scattering mechanism such as constructive interference of the scattered light. At higher particle concentrations, there may be a higher constructive interference that acts to increase the inscattering of light at a specific location due to the multiple number of sites. In Fig. 11C, the model overpredicted the wastewater effluent augmented with particles. One possible reason for the higher model results is due to the type and size of particles in the augmented wastewater solution. The augmented wastewater effluent contains irregular, 2–5 μm particles that may scatter light anisotropically.[25] The anisotropic nature of the scattered light was not modeled in this study. Moreover, modeling the anisotropic nature of the scattered light is complex, involving additional equations that include one or more empirical constants. The empirical nature of the constants in the anisotropic scattering equations makes it difficult to use universally for all large particles and to be specific for the particle-laden solution. However, the results in Fig. 11 suggest that an anisotropic scattering model such as Mie or Rayleigh[25] should be explored when particles in wastewater effluent are modeled.

7. Concluding Remarks

On the basis of the results of this study, the penetration of germicidal UVC irradiance depends on the scattering properties of particles and water absorbance. Moreover, the efficiency of light penetration and subsequently UV disinfection in reactors decreases with an increase in absorbance of dissolved and particulate components in water. Scattering should be incorporated into evaluations of unfiltered water and wastewater effluents used for disinfection
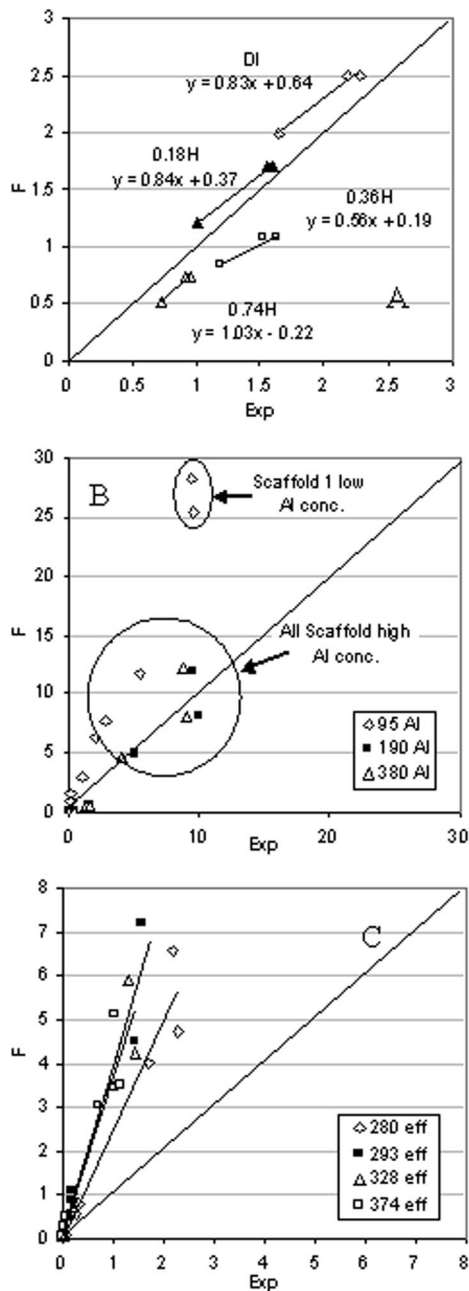
Fig. 11. Comparison between RTE fluence rate model predictions (F) and experimental data (Exp): A, scaffold 2 humics with no particles; B, all scaffolds alumina particles; C, all scaffolds for wastewater effluent augmented with MLSS particles.

to more accurately reflect the true absorbance physics experienced in a UV disinfection system. The initial hypothesis that spherical actinometry is an adequate tool to quantify the effect of particle scattering in UV reactors was validated. The hypothesis that path length of light with scattering suspensions will no longer correspond to the actual cell path length was validated as well. The RTE fluence rate model nearly predicted the behavior of absorbing media devoid of particles and highly scattering particles at elevated concentrations. However, the model did

not well predict natural particle scattering consisting of both absorbing media and particles with jointly absorbing and scattering characteristics.

The UV fluence rate in a scattering and absorbing medium is not simply an average of the fluence rate of the individual scattering and absorbing components. Light scattering by particles is an important parameter to quantify to accurately determine absorbance in turbid media. UV scattering can also provide a possible mechanism to increase the fluence rate and photon path length. This is relevant if UV energy is being wasted and absorbed at the wall of the UV disinfection system. Thus intentional addition of scattering particles to a medium can modify the absorption behavior of the system. This addition of highly scattering submicrometer or nanoparticles to a UV reactor may enhance disinfection, but measures should be taken to remove them postdisinfection to avoid any health implications.

References

1. M. I. Cabrera, O. M. Alfano, and E. Cassano, "Absorption and scattering coefficients of titanium dioxide particulates suspensions in water," J. Phys. Chem. **100,** 20043–20050 (1996).
2. F. J. Loge, R. W. Emerick, M. Heath, J. Jacangelo, G. Tchobanoglous, and J. L. Darby, "Ultraviolet disinfection of secondary wastewater effluents: prediction of performance and design," Water Environ. Res. **68,** 900–916 (1996).
3. K. G. Linden and J. L. Darby, "Ultraviolet disinfection of marginal effluents: determining ultraviolet absorbance and subsequent estimation of ultraviolet intensity," Water Environ. Res. **70,** 214–223 (1998).
4. Y. Du and J. Rabani, "Determination of quantum yields in two-dimensional scattering systems," Photochem. Photobiol. **162,** 575–578 (2004).
5. H. B. Wright, "Comparison and validation of UV dose calculations for low and medium pressure mercury arc lamps," Water Environ. Res. **72,** 439–443 (2000).
6. M. I. Stefan, R. O. Rahn, and J. R. Bolton, "Use of iodide/iodate actinometer together with spherical cells for determination of the fluence rate distribution in UV reactors: validation of the mathematical model," in *Proceedings of the First International Congress on Ultraviolet Technologies* (International Ultraviolet Association, 2001).
7. S. Tassan and K. Allali, "Proposal for the simultaneous measurement of light absorption and backscattering by aquatic particulates," J. Plankton Res. **24,** 471–479 (2002).

8. R. G. Qualls, M. P. Flynn, and D. Johnson, "The role of suspended particles in ultraviolet disinfection," J. Water Pollut. Control Fed. **55,** 1280–1285 (1983).

9. S. Tassan and G. M. Ferrari, "Variability of light absorption by aquatic particles in the near-infrared spectral region," Appl. Opt. **42,** 4802–4810 (2003).

10. J. Christensen and K. G. Linden, "How particles affect UV light in the UV disinfection of unfiltered drinking water," J. Am. Water Works Assoc. **95,** 179–189 (2003).

11. H. Mamane and K. G. Linden, "Impact of particle aggregated microbes on UV disinfection. II: Proper absorbance measurement for UV fluence," ASCE J. Environ. Eng. (to be published).

12. N. B. Nelson and B. B. Prezelin, "Calibration of an integrating sphere for determining the absorption coefficient of scattering suspensions," Appl. Opt. **32,** 6710–6717 (1993).

13. E. Castiglioni and P. Albertini, "An integrating sphere to measure CD from difficult samples," Chirality **12,** 291–294 (2000).

14. C. F. Bohren and D. R. Huffman, *Absorption and Scattering of Light by Small Particles* (Wiley-Interscience, 1983).

15. E. Huber and M. Frost, "Light scattering by small particles," J. Water Supply Res. Technol. Aqua **47,** 87–94 (1998).

16. L. Davydov and P. G. Smirniotis, "Quantification of the primary processes in aqueous heterogeneous photocatalysis using single-stage oxidation reactions," J. Catal. **191,** 105–115 (2000).

17. R. O. Rahn, P. Xu, and S. L. Miller, "Dosimetry of room-air germicidal (254 nm) radiation using spherical actinometry," Photochem. Photobiol. **70,** 314–318 (1999).

18. J. R. Bolton, *Ultraviolet Application Handbook,* 2nd ed. (Bolton Photosciences, 2001).

19. J. Jortner, R. Levine, M. Ottonlenghi, and G. Stein, "The photochemistry of the iodide ion in aqueous solution," J. Phys. Chem. **65,** 1232–1238 (1961).

20. R. O. Rahn, "Potassium iodide as a chemical actinometer for 254 nm radiation: use of iodate as an electron scavenger," Photochem. Photobiol. **66,** 450–455 (1997).

21. S. Jin and K. G. Linden, "Determination of fluence rate distribution in UV reactors using spherical actinometry and mathematical analysis approaches," in *Proceedings of Water Quality Technology Conference* (American Water Works Association, 2002).

22. S. Jin, "Fluence measurements for polychromatic UV disinfection systems: bench scale modeling and application to characterization of UV reactors," Ph.D. dissertation (Duke University, Durham, N.C., 2003).

23. D. Liu, J. J. Ducoste, S. Jin, and K. G. Linden, "Evaluation of alternative fluence rate distribution models," J. Water Supply Res. Technol. Aqua **53,** 391–408 (2004).

24. American Public Health Association, American Water Works Association, and Water Environment Federation, *Standard Methods for the Examination of Water and Wastewater,* 19th ed. (1995).

25. M. F. Modest, *Radiative Heat Transfer* (McGraw-Hill, 1993).

26. J. C. Chai, H. S. Lee, and S. V. Patankar, "Finite volume method for radiation heat transfer," J. Thermophys. Heat Transfer **8,** 419–425 (1994).

27. K. Stamnes, S. C. Tsay, W. Wiscombe, and K. Jayaweera, "Numerically stable algorithm for discrete ordinate method radiative transfer in multiple scattering and emitting media," Appl. Opt. **27,** 2502–2509 (1988).

28. B. T. Liou and C. Y. Wu, "Radiative transfer in a multi-layer medium with Fresnel interfaces," Heat Mass Transfer **32,** 103–107 (1996).

29. L. Passantino, J. Malley, M. Knudson, R. Ward, and J. Kim, "Effect of low turbidity and algae on UV disinfection performance," J. Am. Water Works Assoc. **96,** 128–137 (2004).

30. U.S. Environmental Protection Agency, "Ultraviolet disinfection guidance manual (draft)," EPA 815-D-03-007 (Office of Water, 2003).

31. W. A. Fiveland, "Discrete ordinates solutions of the radiative transport-equation for rectangular enclosures," J. Heat Transfer **106,** 699–706 (1984).